Tissue and Cell 88 (2024) 102369

Contents lists available at ScienceDirect

Tissue and Cell

journal homepage: www.elsevier.com/locate/tice

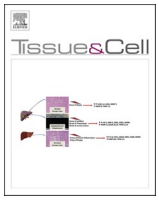

Antioxidant and anti-ageing effects of oleuropein aglycone in canine skeletal muscle cells

Giulia Polacchini, Andrea Venerando, Monica Colitti *

Department of Agricultural, Food, Environmental and Animal Sciences, University of Udine, Italy

ARTICLE INFO

Keywords:
Skeletal muscle cells
Dog
ROS
Ageing
Oleuropein aglycone

ABSTRACT

Reactive oxygen species (ROS) are normally produced in skeletal muscle. However, an imbalance in their regulatory systems can lead to their accumulation and ultimately to oxidative stress, which is one of the causes of the ageing process. Companion dogs share the same environment and lifestyle as humans, making them an excellent comparative model for the study of ageing, as well as they constitute a growing market for bioactive molecules that improve the quality of life of pets. The anti-ageing properties of oleuropein aglycone (OLE), a bioactive compound from olive leaves known for its antioxidant properties, were investigated in Myok9 canine muscle cell model. After incubation with OLE, senescence was induced in the canine cellular model by hydrogen peroxide (H_2O_2). Analyses were performed on cells after seven days of differentiation. The oxidative stress induced by H_2O_2 treatment on differentiated canine muscle cells led to a significant increase in ROS formation, which was reduced by OLE pretreatment alone or in combination with H_2O_2 by about 34% and 32%, respectively. Cells treated with H_2O_2 showed a 48% increase the area of senescent cells stained by SA-β-gal, while OLE significantly reduced the coloured area by 52%. OLE, alone or in combination with H_2O_2, showed a significant antioxidant activity, possibly through autophagy activation, as indicated by the expression of autophagic markers.

1. Introduction

Ageing is a complex natural and biological process that impairs the body's ability to maintain effective metabolic processes and increases the likelihood of disease. The aetiology of ageing is multifactorial and is characterised by inadequate protein intake, increased protein catabolism, increased release of inflammatory cytokines, mitochondrial dysfunction and diffuse oxidative stress (Romani et al., 2022). In skeletal muscle, ageing is characterised by a progressive and general loss of muscle mass and strength. Physiologically, large amounts of reactive oxygen species (ROS) are generated during muscle contraction, making skeletal muscle susceptible to oxidative stress and cellular senescence, especially in the older people (McArdle et al., 2002). Although low levels of ROS are necessary for physiological homeostasis, excessive accumulation of ROS can lead to cellular damage at the molecular level and promote the ageing process (Du et al., 2019; Iakovou and Kourti, 2022).

Domesticated dogs are increasingly recognised as suitable models for a range of biomedical research areas, as they have clear advantages over other commonly used laboratory animals (Hoffman et al., 2018). Dogs that live with their owners are kept into old age and typically receive a high level of care, including nutritional care, resulting in $326 per household being spent annually on canine healthcare (US AVMA, 2022). By modelling the human condition, complex issues such as the contribution of the environment as well as the impact of ageing on disease susceptibility and progression can be investigated with long-term treatment protocols in dogs (Creevy, et al., 2016; Creevy et al., 2022).

In old dogs, skeletal muscle wasting, and frailty are not well studied, but the first clearly visible signs are fatigue and lack of mobility (Freeman, 2012). As in humans, the decline in muscle function in ageing dogs is attributed to oxidative damage to lipids, proteins and DNA that accumulates over time (Mecocci et al., 1999). Reduced expression of genes related to cell cycle and metabolism has been observed in geriatric dogs compared to young adults, suggesting reduced cell turnover and impaired mitochondrial function and dynamics due to fission and fusion processes (Middelbos et al., 2009). As in humans, the expression of the mitochondrial electron transport chain in dogs shows a general deterioration with age (Zahn et al., 2006).

Several studies suggest that autophagy and mitophagy are protective

* Corresponding author.
E-mail address: monica.colitti@uniud.it (M. Colitti).

https://doi.org/10.1016/j.tice.2024.102369
Received 22 January 2024; Received in revised form 26 March 2024; Accepted 27 March 2024
Available online 29 March 2024

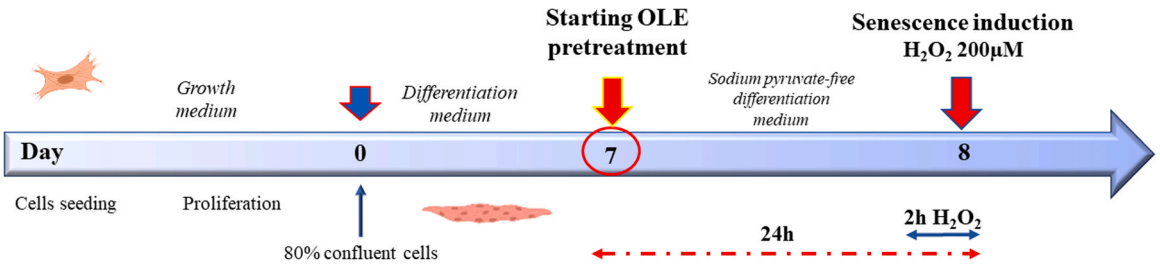

Fig. 1. Experimental design. The cells were 80% confluent and differentiated for 7 days. From day 7 the different treatments started for 24 h and after 22 h the cells in the respective group were exposed to 200 μM H_2O_2 for 2 h to induce oxidative stress and senescence.

mechanisms that maintain muscle health and prevent muscle loss and sarcopenia (Bagherniya et al., 2018) by removing dysfunctional organelles and poorly functioning mitochondria (Lee and Wei, 2012; Sándor and Kubinyi, 2019). In this context, numerous bioactive compounds, such as nutraceuticals found in some foods, can modulate the senescence process (Gurău et al., 2018), and for this reason they have been proposed as suitable anti-ageing molecules. Oleuropein is a natural polyphenol extracted from dried olive leaves. Oleuropein has been shown to have anti-inflammatory, anti-cancer, cardio-protective and neuroprotective properties (Sun et al., 2017; Rishmawi et al., 2022). According to Rigacci et al. (2015), oleuropein also shows antioxidant and anti-ageing effects, which are mainly mediated by the increase in AMPK phosphorylation and thus the inhibition of mTOR signalling, leading to the induction of autophagy (Kucukgul et al., 2020). Interestingly, under oxidative stress conditions, oleuropein acts as an antioxidant at lower doses, while high concentrations of oleuropein show antiproliferative and pro-apoptotic activity as observed in HEY and MCF-7 cells (Scicchitano et al., 2023).

The aim of this study was to test the antioxidant and autophagy-inducing effects of oleuropein aglycone (OLE) on immortalised canine skeletal muscle cells (Myok9) with regard to its efficacy as a pretreatment of a hydrogen peroxide (H_2O_2)-induced senescence stimulus simulating an environmental factor that induces oxidative stress.

2. Material and methods

2.1. Chemicals and culture media

Dulbecco's modified Eagle medium (DMEM)-high glucose (4.5 g/L), GlutaMAX™ Supplement, fetal bovine serum (FBS), sodium pyruvate, penicillin/streptomycin solution (1:1), horse serum, fluorescein anti-rabbit antibody and RIPA lysis buffer, TRIzol reagent, PureLink™ RNA Mini Kit, Platinum™ SYBR™ Green qPCR SuperMix-UDG kit for Real Time-PCR and Hoechst dye were purchased from Life Technologies and Invitrogen (Thermo Fisher Scientific Inc., MA, USA). ImProm-II™ Reverse Transcription System was acquired from Promega (Madison, WI). Oleuropein aglycone (OLE) was purchased from CliniSciences Group (Nanterre, France) and stored in DMSO (EuroClone S.p.A., Milan, Italy). Rapamycin (RAPA), chloroquine diphosphate salt (CLQ), fluorescent probe 2′,7′-dichlorofluorescein diacetate (DCFH-DA), human collagen type I solution and Bradford reagent were purchased by Sigma-Aldrich (Merck KGaA, Darmstadt, Germany). RAPA and CLQ were stored in DMSO and deionised and distilled water (ddH_2O), respectively.

2.2. Cell culture and treatments

Myok9 cells were purchased from ABM Inc. (Richmond, Canada). Cells on the 6th passage were seeded on 0.2% human collagen type I-coated supports (6×10^4 cells for 96-well plate, 10×10^4 for μ-slide 8 well ibiTreat chamber) and were cultured in growth medium (GM) composed of Dulbecco's modified Eagle medium (DMEM) high glucose (4.5 g L^{-1})f supplemented with 2 mM GlutaMAX™, 20% (v/v) fetal bovine serum (FBS), 2% (v/v) chicken embryo extract (VWR International Avantor Inc., PA, USA), 1% (v/v) sodium pyruvate, 100 U mL^{-1} penicillin, and 100 mg mL^{-1} streptomycin at 37°C in humidified 5% (v/v) CO_2 atmosphere. At 80% cell confluence, differentiation was induced by medium replacement with differentiation medium (DM) composed of DMEM-high glucose, 2 mM GlutaMAX™, 1% (v/v) sodium pyruvate, 100 U mL^{-1} penicillin, and 100 mg mL^{-1} streptomycin enriched with 2% (v/v) horse serum (López et al., 2020). Differentiation was carried out for 1 (D1), 4 (D4), and 7 (D7) days.

To avoid the antioxidant effect of sodium pyruvate, each treatment was performed in sodium pyruvate-free DM (Babich et al., 2009). After 7 days of differentiation, cells treated with the same amount of vehicle (0.05% DMSO) were used as control (CTRL). Cells were treated with different concentrations of OLE (10, 25 or 50 μM) and H_2O_2 (100, 200 or 300 μM) in 0.05% DMSO to determine the best concentration to use in the experimental setup without affecting cell viability. To detect autophagy, cells were incubated for 24 hours with 500 nM rapamycin (RAPA), which was used as a positive control and 10 μM chloroquine (CLQ), which targets late-stage autophagy by preventing the fusion of autophagosomes with lysosomes and is able to accumulate LC3B-II protein (Fourrier et al., 2021). In the experimental design Myok9 cells were pretreated with OLE for 22 hours and then exposed to H_2O_2 for 2 hours to induce a senescence stimulus (Fig. 1).

2.3. Immunofluorescence microscopy

Myok9 cells at D1, D4 and D7 were seeded in μ-slide 8 well IbiTreat chamber (Ibidi GmbH, Germany), grown and differentiated as described above. At each time point, cells were fixed with 4% paraformaldehyde (PFA) for 15 min at RT. Fixative-induced autofluorescence was quenched with 50 mM ammonium chloride. Cells were then permeabilized by incubation for 10 min at RT with 0.1% Triton X-100 in phosphate buffered saline (PBS), followed by three washes with PBS. Background labelling was prevented by incubating cells in blocking solution containing 5% (w/v) bovine serum albumin (BSA) and 5% (v/v) normal goat serum (Vector Laboratories, Burlingame, CA) for 1 hours at RT. Fixed cells were incubated at 4°C overnight with rabbit anti-α tubulin primary antibody (1 μg mL^{-1}) (Abcam, Cambridge, UK) dissolved in 1% (w/v) BSA in PBS. After three washes with PBS, cells were incubated for 45 min at RT with secondary fluorescein-conjugated anti-rabbit antibody diluted in 1% (w/v) BSA in PBS. Finally, nuclei were stained with Hoechst dye (1:200 in PBS) for 10 min.

The images were acquired with the Axio Observer Z1 fluorescence microscope equipped with D-PLAN Neofluar objectives with N.A. 0.75 and Infinity Colour Corrected System (ICS) as well as AxioCam and Zen blue software (Carl Zeiss, Jena, 208 Germany). The filters were set to 470/525 nm for 209 fluorescein antibody and 390/460 nm for Hoechst dye. Images were analysed using ImageJ 1.53r software (imagej.nih.gov/ij/).

2.4. Cell viability assay

Cell viability was determined using the 3-(4,5-dimethylthiazol-2-yl)-2,5-diphenyltetrazolium bromide (MTT) assay. Myok9 cells were seeded

Table 1
Oligonucleotide primer sequences for Real Time-PCR (ACTB; β-actin; B2M; β-2-microglobulin; MEF2A; myocyte enhancer factor 2A; MYMK; myoblast fusion factor; SOD2; superoxide dismutase 2; SESN1; sestrin1; PPARGC1A; peroxisome proliferator-activated receptor γ coactivator1α).

Gene	GeneBank accession	Primer sets	Product length (bp)	T_m (°C)
ACTB	Z70044.1	Forward: 5′-ACTGGGACGACATGGAGAAG-3′ Reverse: 5′-AGGGCGTACCCCTCATAGAT-3′	280	59.4
B2M	NM_001284479.1	Forward: 5′-CCTTGCTCCTCATCCTCCTC-3′ Reverse: 5′-GGCTTTCCATTCTCTGCTGG-3′	104	59.4
MEF2A	XM_038661203.1	Forward: 5′-GTCTTTCCCATCCCAAGTGC-3′ Reverse: 5′-AGCTCCCTCTCTGTTTTCCC-3′	90	59.4
MYMK	XM_022423637.2	Forward: 5′-CACACACACACTCATGCACA-3′ Reverse: 5′-GGAGATGTCAGGTGCTCAGA-3′	98	58.4
SOD2	XM_038654563.1	Forward: 5′-CTAAGGGTGGTGGAGAACCA-3′ Reverse: 5′-AAGCGTCCCTGCTCCTTATT-3′	157	58.4
SESN1	NM_014454.3	Forward: 5′-CACACATTCAGACCTCCTTC-3′ Reverse: 5′-TGTAACTGCCTCATCTTTTCC-3′	161	56.6
PPARGC1A	NR_148985.2	Forward: 5′-GCCCAGGTACAGTGAGTCTT-3′ Reverse: 5′-GTGAGGACTGAGGACTTGCT-3′	105	59.8

Tm = annealing temperature

in 96-well plate, differentiated for 7 days and treated as indicated. After treatment, cells were rinsed with PBS and incubated with 5 mg/mL MTT in PBS for 4 h at 37°C. The resulting formazan was dissolved in DMSO and incubated overnight (O/N) at 37°C. Absorbance was measured at λ=570 nm by Spark microplate reader (Tecan Group Ltd., Switzerland).

2.5. Measurement of total intracellular reactive oxygen species (ROS) levels

ROS were estimated using the fluorescent probe DCFH-DA that crosses cell membranes and it is hydrolysed to nonfluorescent DCFH by intracellular esterase. In presence of ROS, DCFH is rapidly oxidized to fluorescent dichlorofluorescin (DCF) that reflects the amount of total intracellular ROS formed.

Myok9 cells were cultured in a 96-well plate, differentiated for 7 days and treated according to the experimental protocol. Prior to H_2O_2 treatment, the plates were incubated in the dark with 30 μM DCFH-DA for 30 minutes at 37 °C. The cells were then treated with H_2O_2 and, after washing with PBS, the fluorescence intensity was measured at 37°C with an excitation wavelength of 485 nm and an emission wavelength of 530 nm using the Spark microplate reader. ROS production was calculated as an increase in fluorescent signal in comparison to CTRL, while the antioxidant activity was calculated as a reduction in fluorescent signal in comparison to the H_2O_2-treated sample.

2.6. SA-β-galactosidase (SA-β-gal) senescence assay

Senescence induction or anti-ageing effect was assessed using the SA-β-gal staining test, in which the blue colour indicates senescent cells. Myok9 cells were seeded in μ-slide 8 well IbiTreat chamber and differentiated for 7 days. Cells were then treated as indicated before incubation with 4% PFA incubation for 15 minutes at RT. After two PBS washes, cells were incubated for 24 hours at 37°C without CO_2 with a freshly prepared SA-β-gal staining solution consisting of 1 μg/mL X-gal, 40 mM citric acid 0.1 M/sodium phosphate 0.2 M solution [pH 6.0], 5 mM potassium ferricyanide, 5 mM potassium ferrocyanide, 150 mM NaCl, and 2 mM $MgCl_2$. The images of the stained cells were acquired with Axio Observer Z1 microscope equipped with the EC-PLAN Neofluar 20x/0.50 M27 objective and the Infinity Colour Corrected System, as well as with the AxioCam 506 camera and Zen blue software (Carl Zeiss, Jena, Germany). The percentage of the blue-coloured area was calculated using ImageJ 1.53r software.

2.7. RNA extraction and Real Time-PCR

To extract RNA from the Myok9 cell cultures, 0.1 mL/cm^2 of TRIzol reagent was added in the Petri dishes after culture medium removal. Then, the collected samples were proceeded with the PureLink™ RNA Mini Kit following the manufacturer's instructions. The concentration of the total RNA extracted was quantified using the acid nucleic quantification tool of the Spark microplate reader. Purity of RNA samples ranged between 1.8 and 1.9.

Primer3 Input software was used to design primers (Rozen and Skaletsky, 2000) for genes related to skeletal muscle differentiation (MEF2A, myocyte enhancer factor 2A; MYMK, myoblast fusion factor; SESN1, sestrin1) and involved in antioxidant defence (SOD2, superoxide dismutase 2; PPARGC1A, peroxisome proliferator-activated receptor γ coactivator1α).

GeneBank accession, primers, product lengths and relative annealing temperatures for each gene are listed in Table 1, according to the HUGO Gene Nomenclature Committee.

Total RNA was reverse-transcribed with the ImProm-II™ Reverse Transcription System (Promega, Madison, WI) in a MJ thermal cycler model PT-100 (MJ Research Inc., USA) following the manufacturer's instructions. Real time PCR analyses were performed in triplicate for each treatment using Platinum™ SYBR™ Green qPCR SuperMix-UDG reaction kit.

For each gene, an aliquot of cDNA samples was pooled and standard curves with serial dilution of the pool were used to optimize Real Time-PCR conditions in terms of cDNA and primers concentration and to calculate the efficiency, fluorescence baseline, and threshold. PCR amplification was achieved applying 40 cycles (10 s at 95°C, 30 s at the specific annealing temperature, 30 s at 72°C) in a 96-well spectrofluorometric thermal cycler CFX (Bio-Rad, Milan, Italy). The melting curve analysis of amplification products was performed at the end of each PCR reaction to confirm that a single PCR product was detected.

Target gene expression was normalised using geometric mean values between β-actin (ACTB) and β-2-microglobulin (B2M) mRNAs and analysed as relative fold change between D4 and D7 compared to D1 using the ΔΔCt method (Livak and Schmittgen, 2001). The relative fold change was also quantified between treatments (H_2O_2, OLE and OLE+H_2O_2) compared to CTRL.

2.8. Cyto-ID fluorescence microscopy autophagy detection assay

The autophagy induction was evaluated by a fluorescence microscopy assay using the Cyto-ID® Autophagy Detection Kit 2.0 (Enzo Life Science, USA) containing a fluorescent probe that marks vesicles produced during the autophagy process (Stankov et al., 2014).

Myok9 cells were seeded in μ-slide 8 well IbiTreat chamber and differentiated for 7 days before being treated as indicated. RAPA treatment was used as positive autophagy controls. After treatment, cells were washed with PBS and stained following the manufacturer's kit protocol. Stained cells were washed with PBS and fixed with 4% PFA for

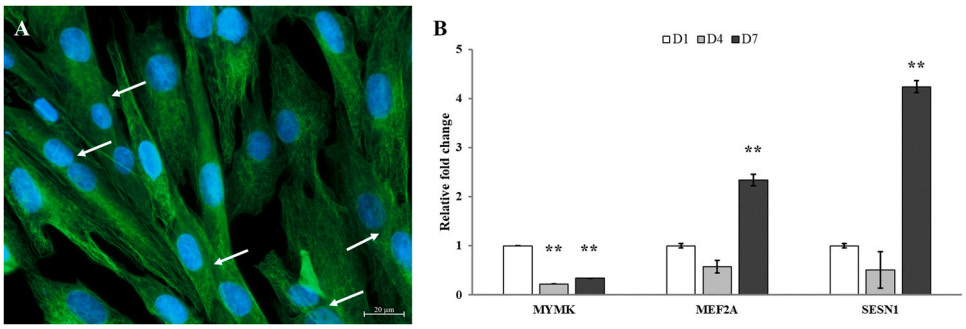

Fig. 2. Characterisation of the differentiation of the Myok9 canine myoblast cell line. (A) Representative image of differentiated Myok9 cells after 7 days. Immunofluorescence of the cytoskeletal protein α-tubulin (green) and nuclear staining with Hoechst dye (blue). The white arrows show fused differentiated cells with more than two nuclei. (B) Gene expression analysis of MYMK, MEF2A and SESN1 in D4 and D7 compared to D1. $^{**}P < 0.01$.

15 min at RT. Images were acquired with the fluorescence microscope Axio Observer Z1. The autophagy vesicles number were counted by ImageJ 1.53r software. Autophagy induction was indicated as an increase in the vesicles number in comparison to CTRL.

2.9. Total protein extraction and western blot analysis

Seven-day differentiated Myok9 cells were detached from the Petri dishes (Ø 10 cm) with a scraper and collected in PBS. To extract total proteins, the cells were lysed in RIPA buffer containing a protease inhibitor cocktail (Roche, Switzerland) as well as 1 mM sodium orthovanadate and sodium fluoride to inhibit phosphatases. The protein concentrations of the samples were determined using the Bradford colorimetric method and the absorbance was measured at 595 nm using the Spark microplate reader (Tecan Group Ltd., Switzerland).

Equal amounts of proteins from each sample (40 µg) were loaded and separated by Tris-glycine-SDS-PAGE. Then, proteins were transferred to PVDF membranes (Immobilon-P; Millipore, Darmstadt, Germany) using the semi-dry Biometra Fastblot apparatus (Analytik Jena GmbH+Co, Jena, Germany). The membranes were incubated overnight at 4°C with primary antibodies diluted in 1% (w/v) bovine serum albumin in Tris-buffered saline (TBS) with 0.1% (w/v) Tween 20. The primary antibodies used were rabbit anti-AMPKα (23A3, Cell Signalling); rabbit anti-p-AMPKα(Thr172) (40H9, Cell Signalling); mouse anti-LC3B (SC-376404, Santa Cruz). After overnight incubation, the membranes were rinsed in 0.1% (w/v) Tween 20 TBS and incubated for 1 hour at room temperature with horseradish peroxidase (HRP)-conjugated secondary antibodies. The HRP-conjugated secondary antibodies were IgG goat anti-rabbit IgG (H+L) (170–6515, BioRad) and IgG goat anti-mouse IgG (H+L) (170–6516, BioRad). CLQ was used as a positive control for LC3B-II protein accumulation. Chemiluminescence detection of HRP-conjugated secondary antibodies was performed using ImageQuant LAS 500 (GE Healthcare Life Sciences, Hatfield, UK) and quantified using ImageJ 1.53r software. Mouse β-actin antibody (A2228, Sigma Merck, Darmstadt, Germany) was used as loading control.

2.10. MitoTracker® staining and mitochondrial structure analysis

Myok9 cells were cultured in µ-slide 8 well IbiTreat chamber differentiated for 7 days and treated as indicated. After treatments, cells were incubated with 100 nM MitoTracker® Orange CMTMRos (Thermo Fisher Scientific Inc., USA) for 30 min at 37°C. Stained cells were washed with PBS and fixed with 4% PFA for 15 min at RT. After fixation, cells were rinsed two times with PBS and incubated with Hoechst dye for 10 min at RT.

Images were acquired with the Axio Observer Z1 fluorescence microscope with filter 550/605 nm for MitoTracker® Orange CMTMRos probe and 390/460 nm Hoechst dye.

The adaptive thresholding-based tool Mitochondrial Analyzer and the open-source image analysis platform ImageJ/Fiji were used to quantify mitochondrial morphology on fluorescence microscopy images (Chaudhry et al., 2020). A scale was set for magnification, and after 2D thresholding optimisation, images were set with a block size of 1.350 µm and a C-value of 5.

The number of mitochondria in the image (count), mean area (total area/mitochondria number, μm^2), mean form factor (shape descriptor measuring round to filamentous shape, arbitrary units), mean aspect ratio (shape descriptor measuring elongation, arbitrary units), and mean branch length (indicator of mitochondrial network connectivity normalized to mitochondria count, µm) were evaluated.

2.11. Statistical analyses

All results are presented as means ± SD and were analysed by XLSTAT statistical software (Addinsoft, 2022).

All fluorescence microscopy data were obtained from at least 10 images of two biological replicates for each treatment. Cell viability and percentage ROS content were obtained from at least 8 biological replicates and ratio of protein expression was determined from 5 technical replicates for each treatment. Data were compared using one-way ANOVA with Dunnett's statistical test in comparison to CTRL or H_2O_2-treated cells. Blue X-gal area and autophagy vesicle count data were compared using the two tailed comparisons Mann-Whitney statistical test. Mitochondrial morphology measurements were compared using the Kruskal-Wallis statistical test with Bonferroni correction. Gene expression data are presented as relative fold-change values compared to D1 or CTRL and were analysed using a one-way ANOVA with Dunnett's statistical test.

3. Results

3.1. Morphological characterization and gene expression of Myok9 during differentiation

The Myok9 canine myoblast cell line was morphologically characterised by immunofluorescence to assess its differentiation efficiency and rate. As shown in Fig. 2A, immunostaining of the cytoskeletal protein α-tubulin in combination with Hoechst nuclear dye showed fused, well-differentiated Myok9 cells with more than two nuclei after 7 days. At this time point, the fusion index was calculated as the percentage of differentiation determined by the ratio of the number of cells with more than two nuclei to the total number of cells in each image. The maximum differentiation of Myok9 cells was 29.22 ± 4.49%.

To confirm the differentiation of Myok9 detected by morphological analysis, the gene expression of MYMK, MEF2A and SESN1 was also examined (Fig. 2B). After 4 days of differentiation, only gene expression of MYMK was significantly altered. In particular, the downregulation of MYMK ($P < 0.01$) detected at D4 was maintained up to D7 (Fig. 2B). In

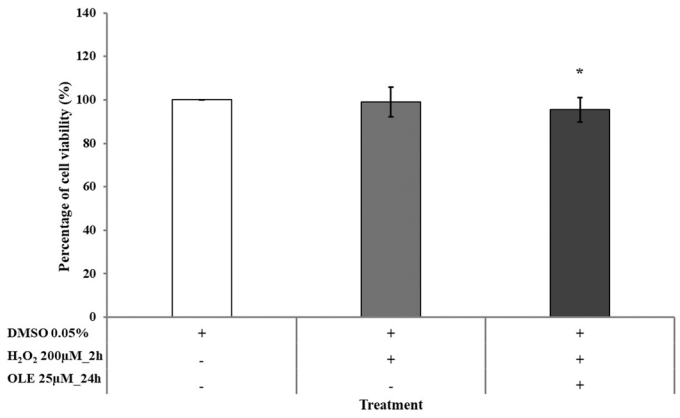

Fig. 3. Effect of combined treatment with OLE and H_2O_2 on the viability of Myok9 cells. Cells were treated with vehicle DMSO 0.05% (CTRL) or H_2O_2 200 µM for 2 h or combined pretreatment with OLE 25 µM and H_2O_2 200 µM for 24 h or 2 h. *$P < 0.05$ *vs* CTRL.

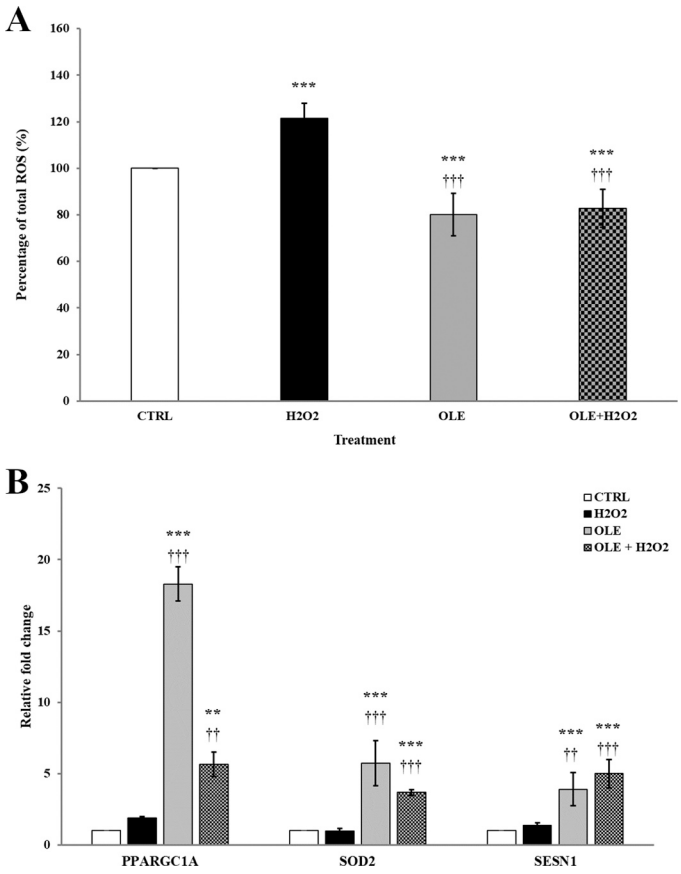

Fig. 4. Antioxidant effect of OLE in differentiated Myok9 cells. (A) Total ROS levels in cells treated with 200 µM H_2O_2, 25 µM OLE or pretreated with 25 µM OLE and then challenged with 200 µM H_2O_2 (OLE+H_2O_2). Cells treated with vehicle (DMSO) were used as control (CTRL). OLE-treated cells showed a significantly lower ROS generation, and this is maintained also after H_2O_2 stimulation. (B) Gene expression analysis of PPARGC1A, SOD2 and SESN1 in H_2O_2-, OLE- and OLE+H_2O_2-treated cells compared to CTRL cells. OLE treatment and pretreatment induce upregulation of the analysed genes. This can explain the decreased ROS generation in OLE-treated and pretreated cells. CTRL, control; H_2O_2 200 µM treated cells; OLE, 25 µM oleuropein-treated cells; OLE+H_2O_2, 25 µM oleuropein-pretreated and H_2O_2 200 µM exposed cells. **$P < 0.01$ *vs* CTRL; ***$P < 0.0001$ *vs* CTRL; ††$P < 0.01$ *vs* H_2O_2; †††$P < 0.0001$ *vs* H_2O_2.

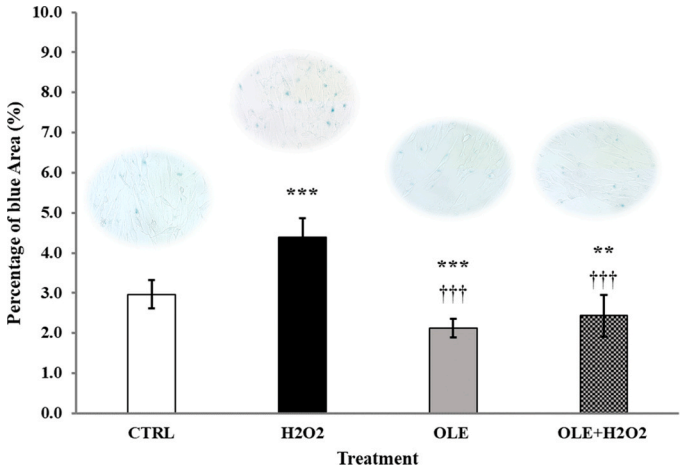

Fig. 5. Anti-senescence activity of OLE in differentiated Myok9 cells. Representative images of SA-β-gal staining and percentage of blue stained area in CTRL and in cells treated with H_2O_2, OLE or OLE+H_2O_2. OLE-treated and pretreated cells show a significant decrease of stained blue area, suggesting a reduction of senescence cells. CTRL, control; H_2O_2 200 µM treated cells; OLE, 25 µM oleuropein-treated cells; OLE+H_2O_2, 25 µM oleuropein-pretreated and H_2O_2 200 µM exposed cells. **$P < 0.01$ *vs* CTRL; ***$P < 0.0001$ *vs* CTRL; †††$P < 0.0001$ *vs* H_2O_2.

contrast, MEF2A and SESN1 gene expression showed no significant changes at D4, while it increased strikingly at D7 ($P < 0.01$) (Fig. 2B).

3.2. Cell viability

A cell viability assay was performed in advance to evaluate the dose- and time-dependent effect of H_2O_2 exposure in differentiated Myok9 cells. Cells were treated with 100, 200 and 300 µM H_2O_2 for 1 and 2 hours. Cell viability (% *vs* CTRL) was reduced at 300 µM H_2O_2 but was still above 90% ($P < 0.001$) at each time point (Fig. S1A). In contrast, 100 µM and 200 µM H_2O_2 did not induce oxidative stress in differentiated Myok9 cells. For this reason, a 2-hour exposure to 200 µM H_2O_2 was chosen to induce oxidative stress without affecting cell viability in our experimental setup.

Differentiated Myok9 cells were also tested with OLE alone or in combination with 200 µM H_2O_2. Concentrations of 25 and 50 µM OLE significantly reduced the percentage of viable cells compared to the untreated control (90.1 ± 6.5% and 73.4 ± 4.1%, respectively) (Fig. S1B). Conversely, OLE at 10 µM did not alter cell viability.

Finally, we tested the combined treatment of different OLE concentrations (10, 25 and 50 µM) with H_2O_2. As shown in Fig. 3, a 24-hour pre-incubation of differentiated Myok9 with 25 µM OLE followed by a 2-hour treatment with 200 µM H_2O_2 significantly reduced cell viability ($P < 0.05$), but maintained it above 95% compared to vehicle (CTRL). Therefore, a 24-hour pretreatment with 25 µM OLE in combination with a 2-hour long exposure to 200 µM H_2O_2 was chosen for the subsequent analyses.

3.3. OLE inhibits H_2O_2-induced ROS formation and increases antioxidant defence system

To evaluate the antioxidant activity of OLE, total ROS formation was quantified in differentiated Myok9 cells. As expected, the ROS production was increased by 22% after H_2O_2 exposure ($P < 0.0001$) (Fig. 4A). In contrast, the percentage of ROS was significantly reduced in OLE- and in OLE+H_2O_2-treated cells compared to CTRL at approximately 20% and compared to H_2O_2 treatment at 34% and 32%, respectively ($P < 0.0001$), indicating that OLE inhibits the production of ROS (Fig. 4A). As the genes PPARGC1A, SOD2 and SESN1 are involved in the defence mechanisms against oxidative stress, their expression was also

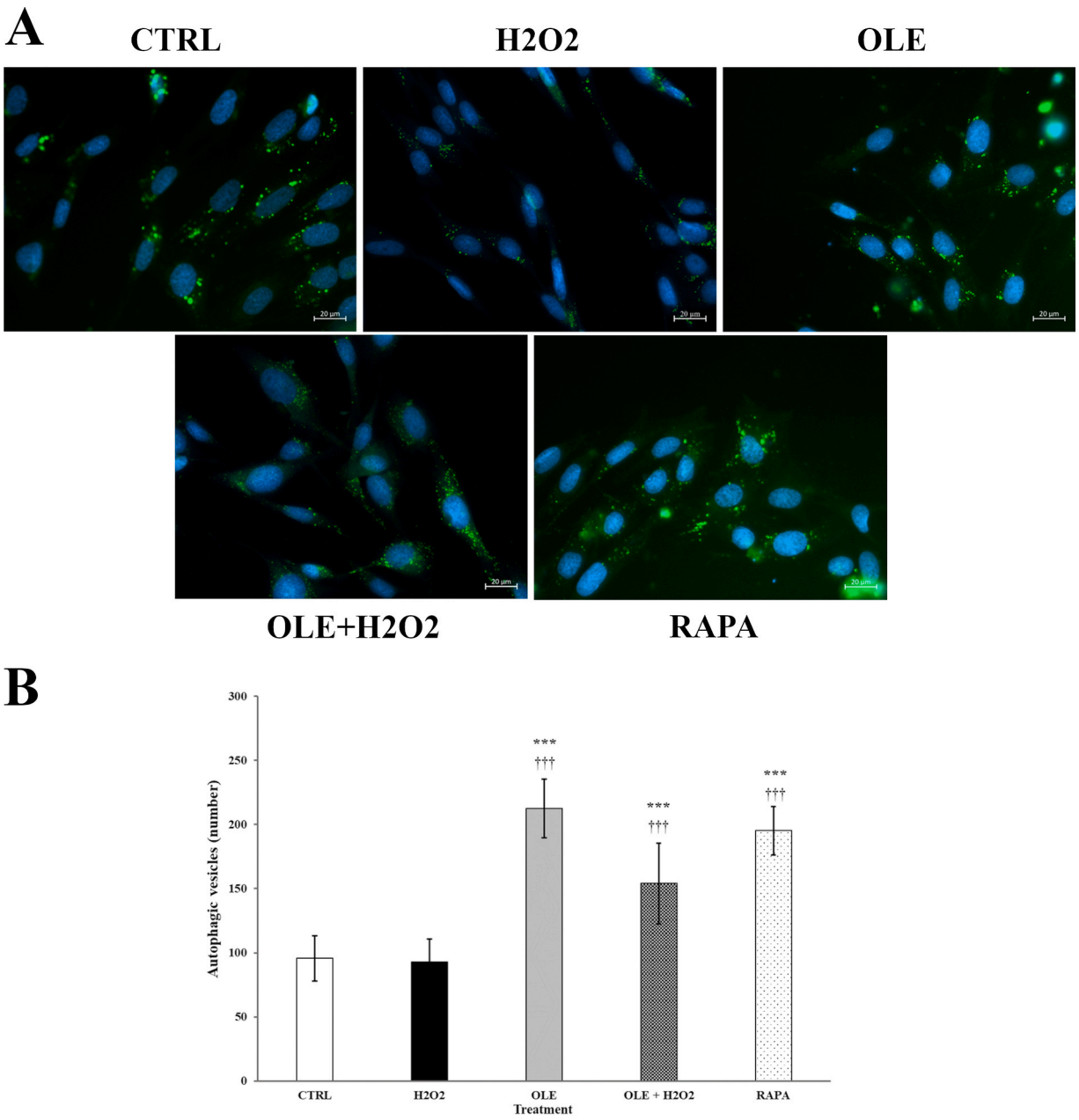

Fig. 6. OLE autophagy induction on differentiated Myok9 cells. (A) Representative images of Cyto-ID fluorescent autophagy vesicles (green) and nuclear staining with Hoechst dye (blue) in CTRL cells and in cells treated with H_2O_2, OLE, OLE+H_2O_2, RAPA. (B) Quantification of autophagic vesicles in CTRL and H_2O_2-exposed cells, in OLE-treated and pretreated cells and in cells treated with RAPA used as positive autophagy control. As in the RAPA, OLE treatment and pre-stimulation significantly increased the number of autophagic vesicles compared to CTRL and H_2O_2 exposed cells. CTRL, control; H_2O_2 200 µM treated cells; OLE, 25 µM oleuropein-treated cells; OLE+H_2O_2, 25 µM oleuropein-pretreated and H_2O_2 200 µM exposed cells; RAPA, 500 nM rapamycin-treated cells. ***$P < 0.0001$ *vs* CTRL; †††$P < 0.0001$ *vs* H_2O_2.

investigated (Fig. 4B). PPARGC1A was significantly upregulated after OLE treatment ($P < 0.0001$) as well as after OLE pretreatment and subsequent H_2O_2 exposure, compared to expression in CTRL and H_2O_2-treated cells ($P < 0.01$) (Fig. 4B). In particular, the expression of PPARGC1A was strongly increased after OLE treatment (up to 18-fold compared to CTRL). This increase in gene expression of members of the antioxidant stress defence apparatus was much less pronounced, albeit significantly upregulated, in cells pretreated with OLE and subsequently exposed to H_2O_2 (Fig. 4B).

3.4. *OLE suppresses the H_2O_2-induced attendance of SA-β-gal*

It has been suggested that the use of antioxidants is an effective approach to preventing symptoms associated with ageing (Gurău et al., 2018). Therefore, to determine whether the antioxidant activity of OLE leads to anti-ageing properties, the presence of the SA-β-gal enzyme, the most commonly used biomarker for senescent and ageing cells, was estimated in differentiated Myok9 cells. In Fig. 5, the blue coloured area, indicating the presence of SA-β-gal, was significantly ($P < 0.0001$) increased by 48% after H_2O_2 incubation compared to CTRL, while it was significantly lower in OLE-treated ($P < 0.0001$) and OLE-pretreated ($P < 0.01$ and $P < 0.0001$) cells than in CTRL and H_2O_2-treated cells, respectively. These results indicate that OLE effectively suppresses H_2O_2-induced SA-β-gal staining in differentiated Myok9 cells by 52%.

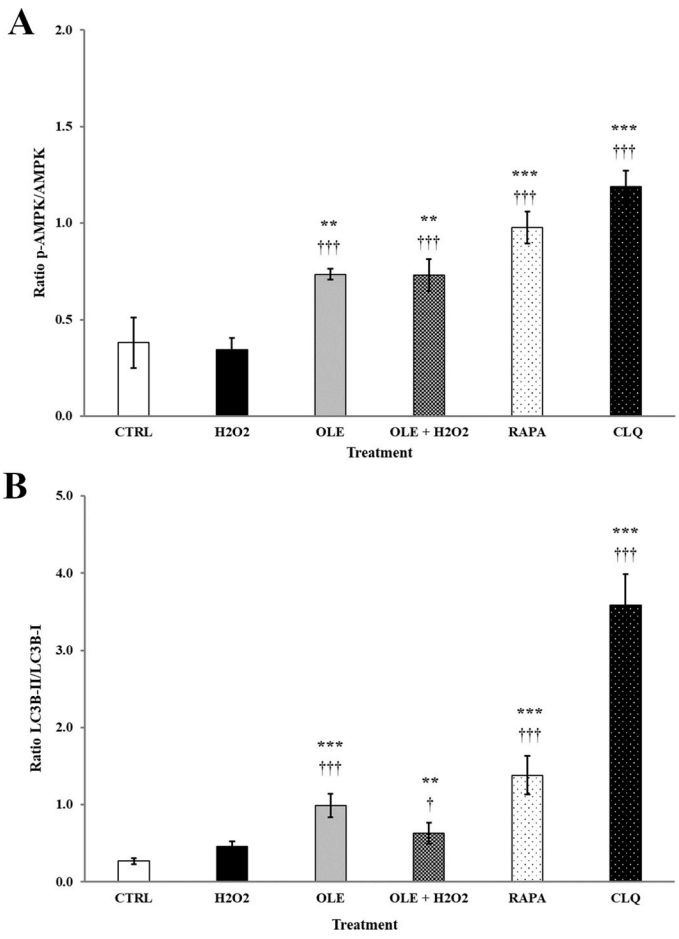

Fig. 7. OLE induces autophagy through AMPKα activation. (A) Ratio of protein expression of p-AMPKα/AMPK in CTRL cells and in cells treated with H_2O_2, OLE, OLE+H_2O_2, RAPA and CLQ. Treatment with OLE and OLE pre-stimulation significantly induces the expression of p-AMPKα. (**B**) Ratio of protein expression of LC3B-I/LC3B-II cells treated as above. The LC3B-I/LC3B-II ratio increased significantly in cells treated with OLE and OLE+H_2O_2 compared to CTRL and H_2O_2-exposed cells as well as in the autophagy-positive control RAPA and CLQ that inhibits autophagic flux. CTRL, control; H_2O_2 200 μM treated cells; OLE, 25 μM oleuropein-treated cells; OLE+H_2O_2, 25 μM oleuropein-pretreated and H_2O_2 200 μM exposed cells; RAPA, 500 nM rapamycin-treated cells; CLQ, 10 μM chloroquine-treated cells. $^{**}P < 0.01$ *vs* CTRL; $^{***}P < 0.0001$ *vs* CTRL; †$P < 0.05$ *vs* H_2O_2; †††$P < 0.0001$ *vs* H_2O_2.

3.5. The anti-ageing effect of OLE is associated with the induction of AMPKα-driven autophagy

Increasing evidence suggests that impaired or reduced autophagy is related to ageing processes (Aman et al., 2021). To test whether the anti-ageing effect demonstrated by OLE is related to the induction of autophagy, the formation of autophagy vesicles in differentiated Myok9 cells was detected using the fluorescence dye Cyto-ID, which specifically labels autophagic compartments, while of lysosomes and endosomes are only minimally stained (Kuk et al., 2023). As shown in Fig. 6A, Cyto-ID fluorescence microscopy images revealed that the number of autophagic vesicles in differentiated Myok9 cells was significantly higher in OLE-treated and pretreated cells compared to CTRL cells and H_2O_2-treated cells, respectively, confirming the stimulatory effect of OLE on the autophagy process (Fig. 6B).

To confirm the ability of OLE to induce autophagy, the expression of two key proteins involved in the core process of autophagy was also analysed, namely the canonical autophagy inducer AMP-activated protein kinase α (AMPKα) and the autophagy marker microtubule-associated protein 1 A/1B-light chain 3 (LC3). Indeed, in differentiated Myok9 cells treated with OLE alone, as well as in cells pretreated with OLE and exposed to H_2O_2, the protein level of AMPKα phosphorylated at threonine 172 (pT172-AMPKα), the active form of AMPKα, was upregulated compared to CTRL- and H_2O_2-exposed cells (Fig. S2 and Fig. 7A).

In addition, the ratio of LC3B-II to LC3B-I was significantly higher in cells incubated with OLE alone and in cells pre-incubated with OLE and then treated with H_2O_2 than in CTRL- and H_2O_2-exposed cells (Figs. S2 and 7B). Similar results were obtained when Myok9 cells were treated with the autophagy inducer RAPA and with CLQ, which inhibits autophagic flux, and enriches LC3B-II (Figs. S2 and 7B). The switch between LC3B-I and LC3B-II, an autophagy marker, and the activation of AMPKα by its phosphorylation at position T172 confirm that the anti-ageing effect of OLE in Myok9 cells is mediated by the induction of the autophagy pathway.

3.6. OLE attenuates the H_2O_2-induced mitochondria fission

In Fig. 8, the dynamic remodelling of mitochondrial morphology by membrane dynamics was investigated using Mitotracker® staining of differentiated Myok9 cells.

The Mitochondrial Analyser tool calculated that the number of mitochondria was significantly higher in cells treated with H_2O_2 than in CTRL cells, and in cells treated with OLE or OLE+H_2O_2. In addition, the mean surface area in H_2O_2-, OLE-treated cells and OLE+H_2O_2-treated cells was significantly lower than in CTRL cells (Fig. 9). Moreover, aspect ratio and form factor, the two major descriptors of mitochondrial shape, were lowest in H_2O_2-treated cells compared to CTRL- and OLE-treated cells, but not in OLE+H_2O_2-treated cells (Fig. 9). Finally, the mitochondrial network, as measured by mean branch length, was lowest in H_2O_2-treated cells and showed a significant difference compared to CTRL cells and cells treated with OLE or OLE-pretreated cells and then challenged with H_2O_2 (Fig. 9).

4. Discussion

The ageing of skeletal muscles leads to frailty and disability, which drastically reduces quality of life (Riuzzi et al., 2018). As life expectancy increases, it is important to understand the mechanisms associated with ageing in order to develop intervention strategies that ensure better quality of life and health in geriatric people. This approach applies to both humans and various animal species, especially companion animals, which represent an increasing elderly animal population in need of veterinary care (Colitti et al., 2019; Day, 2010). In this regard, domestic dogs can rightly be considered the model of choice for the study of ageing, as this species has co-evolved with humans and is exposed to the same environmental conditions such as housing, diet and lifestyle (Mazzatenta et al., 2017; Hoffman et al., 2018). Indeed, dogs are more similar to humans than rodents and can better predict the efficacy of different therapies to prevent the ageing process (Park et al., 2016). However, finding for the best *in vitro* model to study the ageing process and evaluate the appropriate intervention strategies is essential to obtain reliable results that can be translated into clinical practise. For this purpose, Myok9, an already established immortalised canine skeletal muscle cell line (López et al. 2020), was used in the present study.

Although *in vitro* maturation of myoblasts is still a difficult process (Brunetti et al., 2021), canine Myok9 cells showed morphological differentiation after 7 days of differentiation. The maximum percentage of differentiation of Myok9 was 29%, which is consistent with the fusion index of bovine and newborn piglet myoblasts, where it is 30% (Will et al., 2015) and 20% (Mau et al., 2008), respectively. The morphological differentiation of Myok9 was also confirmed by the gene expression of three different genes involved in myoblast differentiation, namely MYMK, MEF2A and SESN1 (Fig. 2B). Indeed, the MYMK gene, which is expressed during myoblast fusion and downregulated

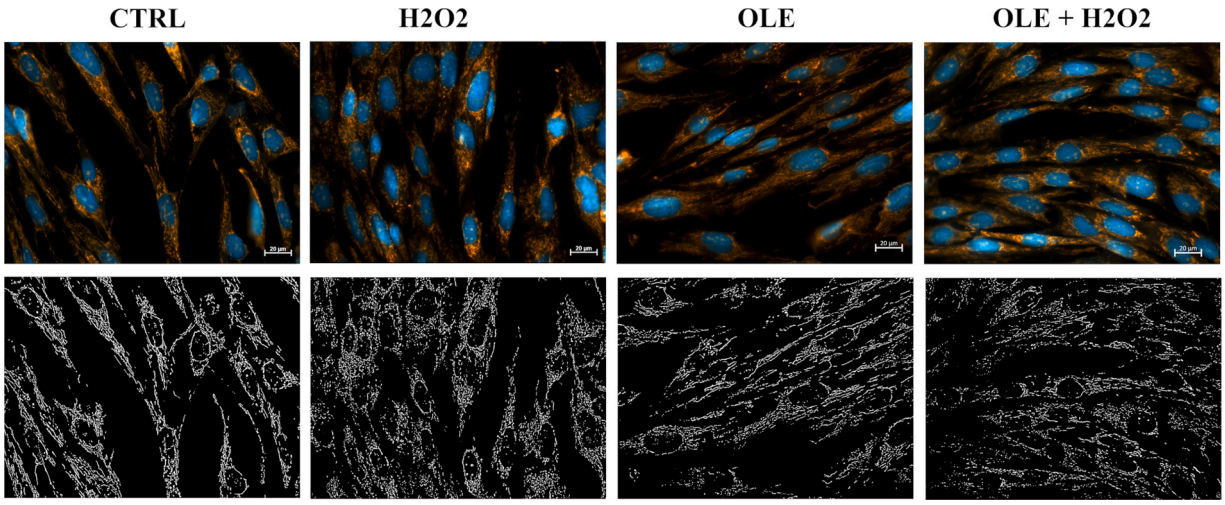

Fig. 8. MitoTracker™ staining of mitochondrial morphology. Representative images of MitoTracker™ and nuclear Hoechst dye staining of treated Myok9 cells and the identification and classification of objects using the adaptive threshold performed with the Mitochondrial Analyser tool. CTRL, control; H_2O_2 200 μM treated cells; OLE, 25 μM oleuropein-treated cells; OLE+H_2O_2, 25 μM oleuropein-pretreated and H_2O_2 200 μM exposed cells.

thereafter (Millay et al., 2013), showed a similar trend in differentiated Myok9 cells. Accordingly, an increase in MEF2A gene expression, which usually accompanies skeletal muscle differentiation (Pon and Marra, 2016), was detected in morphologically differentiated Myok9 cells, as well as the expression of the gene SESN1, which is very low in myoblasts but is strongly induced in differentiated myotubes (Kim et al., 2021).

Oxidative stress is considered one of the main causes of ageing (Schosserer et al., 2018; Diamanti-Kandarakis et al., 2017), and skeletal muscle is particularly vulnerable due to high ROS production during physiological muscle contraction (McArdle et al., 2002). Endogenous ROS overproduction and impaired mitochondrial homeostasis can lead to chronic oxidative stress, which, together with an impaired cell repair system, triggers a senescence process in muscle tissue in older people (Haigis and Yanker, 2010). Several studies have shown that H_2O_2 generates oxidative stress, which in turn causes cell damage and stimulates cell senescence (Sies, 2014; Pomari et al., 2013; Lin et al., 2017). Normally, endogenous antioxidant enzymes catalyse the degradation of free radicals produced in the cells, but the ageing process can be accelerated when ROS levels exceed the capacity of the antioxidant defence system (Negi et al., 2014). In addition, prolonged and severe oxidative stress can also trigger apoptotic signalling and induce cell death (Yüksel et al., 2017). In the present study, H_2O_2 doses were optimised to create an *in vitro* canine muscle cell model for oxidative stress and ageing, by increasing intracellular ROS levels (Fig. 4A) and promoting SA-β-gal detection (Fig. 5), without affecting cell viability.

The use of natural bioactive compounds with antioxidant properties is considered a valuable strategy for the prevention of oxidative stress and thus the prevention of diseases associated with skeletal muscle ageing (Aronson, 2017). OLE is known for its antioxidant, metabolic and anti-inflammatory effects on the liver and skeletal muscle of aged rats (Yoon, 2018; González-Hedström et al., 2021). In addition, OLE showed antiproliferative and pro-apoptotic effects but only at very high concentrations in breast cancer cells (Han et al., 2023). Furthermore, high concentrations of OLE, albeit for very short periods of time, were required to promote antioxidant and anti-ageing effects in human SH-SY5Y neuroblastoma cells (Rigacci et al., 2015). Thus, OLE exerts its effects depending on the cell type, time and concentration of exposure. Overall, the benefit of OLE is considered to be preventive rather than therapeutic (Rishmawi et al., 2022). In the differentiated Myok9 cell model, a longer treatment time of 24 hours with low OLE concentration was used prior to H_2O_2 exposure, creating an *in vitro* condition for oxidative stress. The optimised experimental protocol, which maintains over 95% viability of Myok9 cells (Fig. 3), will be pivotal for potential clinical studies on the effects of OLE in older dogs.

Interestingly, OLE showed antioxidant properties in differentiated Myok9 cells, either when treated directly or when applied 24 hours before the exposure to the oxidative stressor H_2O_2, inhibiting ROS formation (Fig. 4A), thus confirming its role as a promising pharmacological strategy to prevent oxidative damage in muscle tissue. It is noteworthy that the antioxidant activity of OLE has been associated with the activation of various cellular antioxidant defence mechanisms in a variety of cells, such as in human glioblastoma cells, trophoblast cells and in the liver (Rigacci and Stefani, 2016; Kucukgul et al., 2020; Pirković et al., 2023). Indeed, OLE can modulate cellular signalling processes by affecting signal transduction pathways, as previously observed in cultured chicken muscle cells (Muroi et al., 2022) and in aged rats in which supplementation with OLE (100 mg/kg) prevents loss of muscle mass by activating the PI3K/Akt signalling pathway and exerts anti-inflammatory and insulin-sensitising effects on adipose tissue and skeletal muscle (González-Hedström et al., 2021). In the canine Myok9 muscle cell model, both OLE treatment and pretreatment induced the expression of the PPARGC1A, SOD2 and SESN1 genes (Fig. 4B). These findings are consistent with the role of PPARGC1A in skeletal muscle physiology, where its overexpression promotes the mitochondrial biogenic PGC-1α pathway and reduces oxidative damage by regulating cellular oxidant-antioxidant homeostasis (Kang and Li Ji, 2012; Halling and Pilegaard, 2020). Moreover, the upregulation of PPARGC1A is associated with the induction of SOD2 expression, as previously described in rats (Kang et al., 2013). It is noteworthy that OLE treatment, alone or in combination with the H_2O_2 stimulus, affected SESN1 transcription. Sestrins are known as highly conserved stress-responsive proteins that reduce oxidative stress, regulate the mTOR-associated signalling network and prevent muscle atrophy in disuse and ageing (Kim et al., 2021). It should be underlined that although H_2O_2 induces the formation of ROS, it did not significantly alter the expression of these three genes involved in antioxidant activities (Fig. 4B), confirming that the dose and timing of H_2O_2 used in our experimental setup were able to induce oxidative stress without stimulating catalase-mediated detoxification mechanisms (Ransy et al., 2020).

The anti-ageing effect of OLE was previously demonstrated in SH-SY5Y cells where AMPK phosphorylation and subsequent mTORC1 inhibition, induces autophagy (Rigacci et al., 2015). In addition, OLE dietary supplementation has been described to decrease inflammatory status in skeletal muscle, increase mitochondrial biogenesis and improve insulin sensitivity in aged rats (González-Hedström et al., 2021). Recently, OLE was reported to activate a direct mitochondrial Ca^{2+}

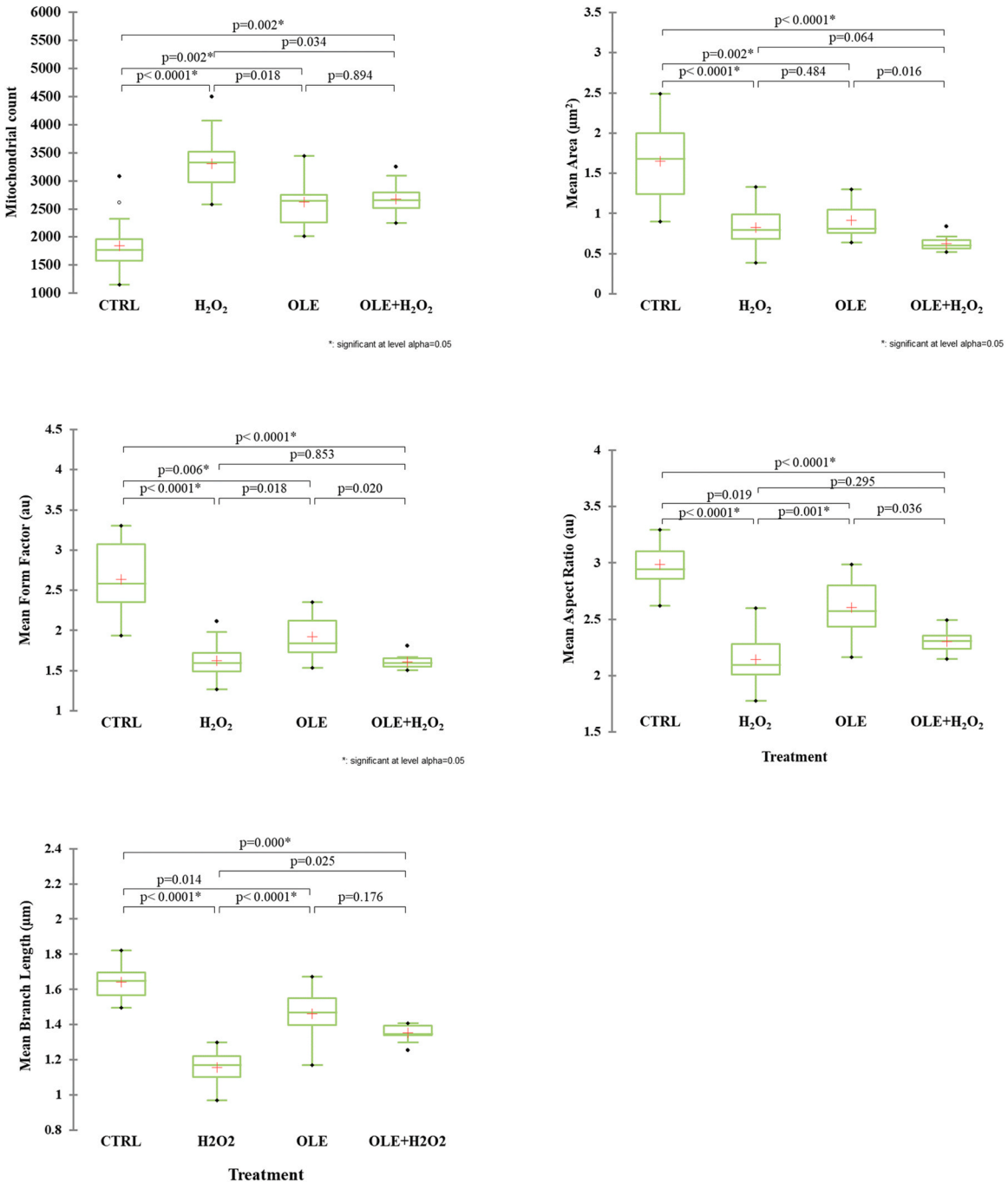

Fig. 9. Quantitative comparison of mitochondrial morphology. Differences in the distribution of mitochondrial morphological features (number of mitochondria, size of mitochondria measured by mean area, shape of mitochondria measured by mean form factor and mean aspect ratio, mitochondrial network measured by mean branching length) were analysed between CTRL cells and cells treated with H_2O_2, OLE and OLE+H_2O_2. Boxplots showed the difference between the medians (horizontal lines), the first to third quartiles (box) and the most extreme values within the interquartile range (vertical lines) between the treatments. The statistical significance in the boxplots was determined by the Kruskal-Wallis statistical test with Bonferroni correction ($P < 0.0083$). CTRL, control; H_2O_2 200 µM treated cells; OLE, 25 µM oleuropein-treated cells; OLE+H_2O_2, 25 µM oleuropein-pretreated and H_2O_2 200 µM exposed cells.

uniporter in skeletal muscle mitochondria that stimulates mitochondrial bioenergetics and muscle performance in aged mice (Gherardi et al., 2021).

In differentiated Myok9 cells, OLE significantly reduced the presence of SA-β-gal (Fig. 5) and stimulated the autophagy process (Fig. 6) both directly and as a preventive agent in cells exposed to an H_2O_2-mediated senescence stimulus. In addition, upregulation of the phosphorylated active form of AMPKα (pT172-AMPKα) and expression of LC3B-II (Fig. 7) confirmed its anti-ageing role in canine muscle cells.

Mitochondria are dynamic organelles that adapt their morphology to the cellular environment and are constantly undergoing fission and fusion (Cadenas and Davies, 2000). Oxidative stress leads to an imbalance between mitochondrial fission and fusion and favours mitochondrial fragmentation (Lee and Wei, 2012; Adebayo et al., 2021), as observed in C2C12 myocytes after exogenous H_2O_2 stimulation (Iqbal and Hood, 2014). In general, mitochondria are elongated, enlarged, and hyperfused in various models of cellular senescence (Lee et al., 2007), suggesting impaired mitophagy (Martini and Passos, 2023). In contrast

Myok9 cells, in our experimental model, showed a significant increase in the number of mitochondria after ROS accumulation, which were smaller, spotted and less interconnected (Fig. 6). Of note, both OLE treatment and pretreatment partially reversed the effects of H_2O_2, probably by inducing SOD2 overexpression. In addition, the increase in PPARGC1A expression promoted by OLE confirmed the activation of the mitochondrial biogenesis process, as reported in detail by Blanco-Benítez et al. (2022), again confirming that OLE may represent an interesting, natural option to counteract oxidative stress. However, further studies are needed to understand the effect of OLE on mitochondrial dynamics.

In conclusion, these results provide new evidence that OLE plays a key role in the prevention of skeletal muscle ageing by acting as an antioxidant compound and promoting autophagy. These findings can be used to develop specific nutritional supplements for dogs as a valuable strategy to prevent age-related muscle diseases that drastically reduce the quality of life of pets.

Fundings

This work was granted by Friulchem S.p.A. (Vivaro, PN Italy) within PhD project titled 'L'utilizzo della nutraceutica e lo studio di alimenti funzionali' PON Ricerca e Innovazione 2014–2020.

CRediT authorship contribution statement

Monica Colitti: Writing – review & editing, Supervision, Project administration, Funding acquisition, Data curation, Conceptualization. **Andrea Venerando:** Writing – review & editing, Formal analysis. **Giulia Polacchini:** Writing – original draft, Methodology, Formal analysis, Data curation, Conceptualization.

Declaration of Competing Interest

All authors declare that they have no conflict of interest.

Data availability

Data will be made available on request.

Appendix A. Supporting information

Supplementary data associated with this article can be found in the online version at doi:10.1016/j.tice.2024.102369.

References

Addinsoft. 2022. XLSTAT statistical and data analysis solution. USA: New York. Available at: https://www.xlstat.com/en (accessed December 18, 2022).

Adebayo, M., Singh, S., Singh, A.P., Dasgupta, S., 2021. Mitochondrial fusion and fission: The fine-tune balance for cellular homeostasis. FASEB J. 35 (6), e21620 https://doi.org/10.1096/fj.202100067R.

Aman, Y., Schmauck-Medina, T., Hansen, M., Morimoto, R.I., Simon, A.K., Bjedov, I., 2021. Autophagy in healthy aging and disease. Nat. Aging 1 (8), 634–650. https://doi.org/10.1038/s43587-021-00098-4.

Aronson, J.K., 2017. Defining 'nutraceuticals': neither nutritious nor pharmaceutical. Br. J. Clin. Pharm. 83 (1), 8–19. https://doi.org/10.1111/bcp.12935.

Babich, H., Liebling, E.J., Burger, R.F., Zuckerbraun, H.L., Schuck, A.G., 2009. Choice of DMEM, formulated with or without pyruvate, plays an important role in assessing the *in vitro* cytotoxicity of oxidants and prooxidant nutraceuticals. Vitr. Cell Dev. Biol. Anim. 45 (5-6), 226–233 doi.org 10.1007/s11626-008-9168-z.

Bagherniya, M., Butler, A.E., Barreto, G.E., Sahebkar, A., 2018. The effect of fasting or calorie restriction on autophagy induction: A review of the literature. Ageing Res. Rev. 47, 183–197. https://doi.org/10.1016/j.arr.2018.08.004.

Blanco-Benítez, M., Calderón-Fernández, A., Canales-Cortés, S., Alegre-Cortés, E., Uribe-Carretero, E., Paredes-Barquero, M., et al., 2022. Biological effects of olive oil phenolic compounds on mitochondria. Mol. Cell Oncol. 9 (1), 2044263. https://doi.org/10.1080/23723556.2022.2044263.

Brunetti, J., Koenig, S., Monnier, A., Frieden, M., 2021. Nanopattern surface improves cultured human myotube maturation. Skelet. Muscle 11 (1), 12. https://doi.org/10.1186/s13395-021-00268-3.

Cadenas, E., Davies, K.J., 2000. Mitochondrial free radical generation, oxidative stress, and aging. Free Radic. Biol. Med 29 (3-4), 222–230. https://doi.org/10.1016/s0891-5849(00)00317-8.

Chaudhry, A., Shi, R., Luciani, D.S., 2020. A pipeline for multidimensional confocal analysis of mitochondrial morphology, function, and dynamics in pancreatic β-cells. Am. J. Physiol. Endocrinol. Metab. 318 (2), E87–E101. https://doi.org/10.1152/ajpendo.00457.2019.

Colitti, M., Stefanon, B., Gabai, G., Gelain, M.E., Bonsembiante, F., 2019. Oxidative stress and nutraceuticals in the modulation of the immune function: current knowledge in animals of veterinary interest. Antioxid. (Basel) 8 (1), 28. https://doi.org/10.3390/antiox8010028.

Creevy, K.E., Akey, J.M., Kaeberlein, M., Promislow, D.E.L., 2022. An open science study of ageing in companion dogs. Nature 602 (7895), 51–57. https://doi.org/10.1038/s41586-021-04282-9.

Creevy, K.E., Austad, S.N., Hoffman, J.M., O'Neill, D.G., Promislow, D.E., 2016. The companion dog as a model for the longevity dividend. Cold Spring Harb. Perspect. Med. 4 6 (1), a026633. https://doi.org/10.1101/cshperspect.a026633.

Day, M.J., 2010. Ageing, immunosenescence and inflammageing in the dog and cat. J. Comp. Pathol. 142 (Suppl 1), S60–S69. https://doi.org/10.1016/j.jcpa.2009.10.011.

Diamanti-Kandarakis, E., Dattilo, M., Macut, D., Duntas, L., Gonos, E.S., Goulis, D.G., et al., 2017. Combo Endo team: 2016. Mechanisms in endocrinology: Aging and anti-aging: a Combo-Endocrinology overview. Eur. J. Endocrinol. 176 (6), R283–R308. https://doi.org/10.1530/EJE-16-1061.

Du, L., Chen, E., Wu, T., Ruan, Y., Wu, S., 2019. Resveratrol attenuates hydrogen peroxide-induced aging through upregulation of autophagy in human umbilical vein endothelial cells. Drug Des. Devel Ther. 13, 747–755. https://doi.org/10.2147/DDDT.S179894.

Fourrier, C., Bryksin, V., Hattersley, K., Hein, L.K., Bensalem, J., Sargeant, T.J., 2021. Comparison of chloroquine-like molecules for lysosomal inhibition and measurement of autophagic flux in the brain. Biochem Biophys. Res Commun. 534, 107–113. https://doi.org/10.1016/j.bbrc.2020.12.008.

Freeman, L.M., 2012. Cachexia and sarcopenia: emerging syndromes of importance in dogs and cats. J. Vet. Intern Med 26 (1), 3–17. https://doi.org/10.1111/j.1939-1676.2011.00838.x.

Gherardi, G., De Mario, A., Mammucari, C., 2021. The mitochondrial calcium homeostasis orchestra plays its symphony: Skeletal muscle is the guest of honor. Int Rev. Cell Mol. Biol. 362, 209–259. https://doi.org/10.1016/bs.ircmb.2021.03.005.

González-Hedström, D., de la Fuente-Fernández, M., Priego, T., Martín, A.I., Amor, S., López-Calderón, A., et al., 2021. Addition of Olive leaf extract to a mixture of algae and extra virgin olive oils decreases fatty acid oxidation and synergically attenuates age-induced hypertension, sarcopenia and insulin resistance in rats. Antioxid. (Basel) 10 (7), 1066. https://doi.org/10.3390/antiox10071066.

Gurău, F., Baldoni, S., Prattichizzo, F., Espinosa, E., Amenta, F., Procopio, A.D., et al., 2018. Anti-senescence compounds: A potential nutraceutical approach to healthy aging. Ageing Res Rev. 46, 14–31. https://doi.org/10.1016/j.arr.2018.05.001.

Haigis, M.C., Yankner, B.A., 2010. The aging stress response. Mol. Cell 40 (2), 333–344. https://doi.org/10.1016/j.molcel.2010.10.002.

Halling, J.F., Pilegaard, H., 2020. PGC-1α-mediated regulation of mitochondrial function and physiological implications. Appl. Physiol. Nutr. Metab. 45 (9), 927–936. https://doi.org/10.1139/apnm-2020-0005.

Han, S., Hou, H., Zhang, Y., Fang, Z., Li, Y., Zhang, L., et al., 2023. Oleuropein and its hydrolysate from extra virgin olive oil inhibit breast cancer cells proliferation interfering with the PI3K-AKT signal pathway. J. Funct. Foods 110, 105880. https://doi.org/10.1016/j.jff.2023.105880.

Hoffman, J.M., Creevy, K.E., Franks, A., O'Neill, D.G., Promislow, D.E.L., 2018. The companion dog as a model for human aging and mortality. Aging Cell 17 (3), e12737. https://doi.org/10.1111/acel.12737.

Iakovou, E., Kourti, M., 2022. A Comprehensive overview of the complex role of oxidative stress in aging, the contributing environmental stressors and emerging antioxidant therapeutic interventions. Front Aging Neurosci. 14, 827900 https://doi.org/10.3389/fnagi.2022.827900.

Iqbal, S., Hood, D.A., 2014. Oxidative stress-induced mitochondrial fragmentation and movement in skeletal muscle myoblasts. Am. J. Physiol. Cell Physiol. 306 (12), C1176–C1183. https://doi.org/10.1152/ajpcell.00017.2014.

Kang, C., Chung, E., Diffee, G., Ji, L.L., 2013. Exercise training attenuates aging-associated reduction in mitochondrial biogenesis in rat skeletal muscle. Exp. Gerontol. 48 (11), 1343–1350. https://doi.org/10.1016/j.exger.2013.08.004.

Kang, C., Li Ji, L., 2012. Role of PGC-1α signaling in skeletal muscle health and disease. Ann. N. Y Acad. Sci. 1271 (1), 110–117. https://doi.org/10.1111/j.1749-6632.2012.06738.x.

Kim, M., Kowalsky, A.H., Lee, J.H., 2021. Sestrins in physiological stress responses. Annu Rev. Physiol. 83, 381–403. https://doi.org/10.1146/annurev-physiol-031620-092317.

Kucukgul, A., Isgor, M.M., Duzguner, V., Atabay, M.N., Kucukgul, A., 2020. Antioxidant effects of Oleuropein on Hydrogen Peroxide-induced neuronal stress- An *In Vitro* Study. Antiinflamm Antiallergy Agents Med Chem. 19 (1), 74–84. https://doi.org/10.2174/1871523018666190201145824.

Kuk, M.U., Lee, H., Song, E.S., Lee, Y.H., Park, J.Y., Jeong, S., et al., 2023. Functional restoration of lysosomes and mitochondria through modulation of AKT activity ameliorates senescence. Exp. Gerontol. 173, 112091 https://doi.org/10.1016/j.exger.2023.112091.

Lee, H.C., Wei, Y.H., 2012. Mitochondria and aging. Adv. Exp. Med Biol. 942, 311–327. https://doi.org/10.1007/978-94-007-2869-1_14.

Lee, S., Jeong, S.Y., Lim, W.C., Kim, S., Park, Y.Y., Sun, X., et al., 2007. Mitochondrial fission and fusion mediators, hFis1 and OPA1, modulate cellular senescence. J. Biol. Chem. 282 (31), 22977–22983. https://doi.org/10.1074/jbc.M700679200.

Lin, X.L., Liu, Y., Liu, M., Hu, H., Pan, Y., Fan, X.J., et al., 2017. Inhibition of Hydrogen Peroxide-induced human umbilical vein endothelial cells aging by Allicin depends on Sirtuin1 activation. Med Sci. Monit. 23, 563–570. https://doi.org/10.12659/msm.899730.

Livak, K.J., Schmittgen, T.D., 2001. Analysis of relative gene expression data using real-time quantitative PCR and the 2(-Delta Delta C(T)) Method. Methods 25 (4), 402–408. https://doi.org/10.1006/meth.2001.1262.

López, S.M., Balog-Alvarez, C., Canessa, E.H., Hathout, Y., Brown, K.J., Vitha, S., et al., 2020. Creation and characterization of an immortalized canine myoblast cell line: Myok9. Mamm. Genome 31 (3-4), 95–109. https://doi.org/10.1007/s00335-020-09833-5.

Martini, H., Passos, J.F., 2023. Cellular senescence: all roads lead to mitochondria. FEBS J. 290 (5), 1186–1202. https://doi.org/10.1111/febs.16361.

Mau, M., Oksbjerg, N., Rehfeldt, C., 2008. Establishment and conditions for growth and differentiation of a myoblast cell line derived from the semimembranosus muscle of newborn piglets. Vitr. Cell Dev. Biol. Anim. 44 (1-2), 1–5. https://doi.org/10.1007/s11626-007-9069-6.

Mazzatenta, A., Carluccio, A., Robbe, D., Giulio, C.D., Cellerino, A., 2017. The companion dog as a unique translational model for aging. Semin Cell Dev. Biol. 70, 141–153. https://doi.org/10.1016/j.semcdb.2017.08.024.

McArdle, A., Vasilaki, A., Jackson, M., 2002. Exercise and skeletal muscle ageing: cellular and molecular mechanisms. Ageing Res Rev. 1 (1), 79–93. https://doi.org/10.1016/s0047-6374(01)00368-2.

Mecocci, P., Fanó, G., Fulle, S., MacGarvey, U., Shinobu, L., Polidori, M.C., et al., 1999. Age-dependent increases in oxidative damage to DNA, lipids, and proteins in human skeletal muscle. Free Radic. Biol. Med 26 (3-4), 303–308. https://doi.org/10.1016/s0891-5849(98)00208-1.

Middelbos, I.S., Vester, B.M., Karr-Lilienthal, L.K., Schook, L.B., Swanson, K.S., 2009. Age and diet affect gene expression profile in canine skeletal muscle. PLoS ONE 4 (2), e4481. https://doi.org/10.1371/journal.pone.0004481.

Millay, D.P., O'Rourke, J.R., Sutherland, L.B., Bezprozvannaya, S., Shelton, J.M., Bassel-Duby, R., Olson, E.N., 2013. Myomaker is a membrane activator of myoblast fusion and muscle formation. Nature 499 (7458), 301–305. https://doi.org/10.1038/nature12343.

Muroi, Y., Aburaya, I., Shima, T., Matsumoto, M., Sasahara, R., Suzuki, T., et al., 2022. Repression effects of hydrolysates from Hen-Egg proteins on amyloid fibril formation. J. Poult. Sci. 59 (4), 384–391. https://doi.org/10.2141/jpsa.0220038.

Negi, R., Pande, D., Karki, K., Kumar, A., Khanna, R.S., Khanna, H.D., 2014. Association of oxidative DNA damage, protein oxidation and antioxidant function with oxidative stress induced cellular injury in pre-eclamptic/eclamptic mothers during fetal circulation. Chem. Biol. Inter. 208, 77–83. https://doi.org/10.1016/j.cbi.2013.11.010.

Park, J.S., Withers, S.S., Modiano, J.F., Kent, M.S., Chen, M., Luna, J.I., et al., 2016. Canine cancer immunotherapy studies: linking mouse and human. J. Immunother. Cancer 20 (4), 97. https://doi.org/10.1186/s40425-016-0200-7.

Pirković, A., Vilotić, A., Borozan, S., Nacka-Aleksić, M., Bojić-Trbojević, Ž., Krivokuća, M.J., et al., 2023. Oleuropein attenuates oxidative stress in human trophoblast cells. Antioxid. (Basel) 12 (1), 197. https://doi.org/10.3390/antiox12010197.

Pomari, E., Stefanon, B., Colitti, M., 2013. Effect of *Arctium lappa* (burdock) extract on canine dermal fibroblasts. Vet. Immunol. Immunopathol. 156 (3-4), 159–166. https://doi.org/10.1016/j.vetimm.2013.10.008.

Pon, J.R., Marra, M.A., 2016. MEF2 transcription factors: developmental regulators and emerging cancer genes. Oncotarget 7 (3), 2297–2312. https://doi.org/10.18632/oncotarget.6223.

Ransy, C., Vaz, C., Lombès, A., Bouillaud, F., 2020. Use of H_2O_2 to Cause Oxidative Stress, the Catalase Issue. Int J. Mol. Sci. 21 (23), 9149. https://doi.org/10.3390/ijms21239149.

Rigacci, S., Miceli, C., Nediani, C., Berti, A., Cascella, R., Pantano, D., et al., 2015. Oleuropein aglycone induces autophagy via the AMPK/mTOR signalling pathway: a mechanistic insight. Oncotarget 6, 35344–35357. https://doi.org/10.18632/oncotarget.6119.

Rigacci, S., Stefani, M., 2016. Nutraceutical properties of Olive Oil Polyphenols. An itinerary from cultured cells through animal models to humans. Int J. Mol. Sci. 17 (6), 843. https://doi.org/10.3390/ijms17060843.

Rishmawi, S., Haddad, F., Dokmak, G., Karaman, R., 2022. A Comprehensive review on the anti-cancer effects of Oleuropein. Life (Basel) 12 (8), 1140. https://doi.org/10.3390/life12081140.

Riuzzi, F., Sorci, G., Arcuri, C., Giambanco, I., Bellezza, I., Minelli, A., Donato, R., 2018. Cellular and molecular mechanisms of sarcopenia: the S100B perspective. J. Cachex-.-. Sarcopenia Muscle 9 (7), 1255–1268. https://doi.org/10.1002/jcsm.12363.

Romani, P., Nirchio, N., Arboit, M., Barbieri, V., Tosi, A., Michielin, F., et al., 2022. Mitochondrial fission links ECM mechanotransduction to metabolic redox homeostasis and metastatic chemotherapy resistance. Nat. Cell Biol. 24 (2), 168–180. https://doi.org/10.1038/s41556-022-00843-w.

Rozen, S., Skaletsky, H., 2000. Primer3 on the WWW for general users and for biologist programmers. Methods Mol. Biol. 132, 365–386. https://doi.org/10.1385/1-59259-192-2:365.

Sándor, S., Kubinyi, E., 2019. Genetic pathways of aging and their relevance in the dog as a natural model of human aging. Front Genet 10, 948. https://doi.org/10.3389/fgene.2019.00948.

Schosserer, M., Grillari, J., Wolfrum, C., Scheideler, M., 2018. Age-induced changes in white, brite, and brown adipose depots: A Mini-Review. Gerontology 64 (3), 229–236. https://doi.org/10.1159/000485183.

Scicchitano, S., Vecchio, E., Battaglia, A.M., Oliverio, M., Nardi, M., Procopio, A., et al., 2023. The double-edged sword of oleuropein in ovarian cancer cells: from antioxidant functions to cytotoxic effects. Int J. Mol. Sci. 24 (1), 842. https://doi.org/10.3390/ijms24010842.

Sies, H., 2014. Role of metabolic H_2O_2 generation: redox signaling and oxidative stress. J. Biol. Chem. 289 (13), 8735–8741. https://doi.org/10.1074/jbc.R113.544635.

Stankov, M., Panayotova-Dimitrova, D., Leverkus, M., Klusmann, J., Behrens, G., 2014. Flow Cytometric Analysis of Autophagic Activity with Cyto-ID Staining in Primary Cells. Bio-Protoc. 4 (7), e1090 https://doi.org/10.21769/BioProtoc.1090.

Sun, W., Wang, X., Hou, C., Yang, L., Li, H., Guo, J., et al., 2017. Oleuropein improves mitochondrial function to attenuate oxidative stress by activating the Nrf2 pathway in the hypothalamic paraventricular nucleus of spontaneously hypertensive rats. Neuropharmacology 113 (Pt A), 556–566. https://doi.org/10.1016/j.neuropharm.2016.11.010.

US AVMA pet ownership and demographics sourcebook. 2022. American Veterinary Medical Association.

Will, K., Schering, L., Albrecht, E., Kalbe, C., Maak, S., 2015. Differentiation of bovine satellite cell-derived myoblasts under different culture conditions. Vitr. Cell Dev. Biol. Anim. 51 (9), 885–889. https://doi.org/10.1007/s11626-015-9916-9.

Yoon, S.K., 2018. Oleuropein as an antioxidant and liver protect (Pages). : Liver. Oxid. Stress Diet. Antioxid. 323–335. https://doi.org/10.1016/B978-0-12-803951-9.00027-6.

Yüksel, E., Nazıroğlu, M., Şahin, M., Çiğ, B., 2017. Involvement of TRPM2 and TRPV1 channels on hyperalgesia, apoptosis and oxidative stress in rat fibromyalgia model: Protective role of selenium. Sci. Rep. 7 (1), 17543. https://doi.org/10.1038/s41598-017-17715-1.

Zahn, J.M., Sonu, R., Vogel, H., Crane, E., Mazan-Mamczarz, K., Rabkin, R., et al., 2006. Transcriptional profiling of aging in human muscle reveals a common aging signature. PLoS Genet 2 (7), e115. https://doi.org/10.1371/journal.pgen.0020115.